AIAA JOURNAL
Vol. 39, No. 4, April 2001

System Identification and Control Design for a Curved Platelike Active Structure

Amir M. Sadri* and Jan Wright†
Manchester School of Engineering, Manchester, England M13 9PL, United Kingdom
and
Richard Wynne‡
Sheffield Hallam University, Sheffield, England S1 1WB, United Kingdom

Active vibration suppression of a curved plate incorporating two piezoelectric actuators is examined. This structure was chosen as one for which it was assumed that no analytical model could be developed accurately for control design purposes; rather, the aim is to identify a multi-input/multi-output (MIMO) model using Hankel singular value decomposition (HSVD). The measurement model is fitted simultaneously across all of the transfer functions in a MIMO system; therefore, a set of poles common to all of the transfer functions is selected. Different control strategies such as single-input/single-output velocity feedback and MIMO linear quadratic Gaussian (LQG) and H_∞ were designed, implemented, and tested using the model identified. The system was successful in reducing the vibration of the flexible modes of the structure. The major performance limitations were the authority of the piezoelectric actuators and the choice of actuator/sensor complement.

Introduction

WITHIN the past decade an area of increasing interest has been the active and passive control of large, high-performance space-based communications, surveillance and weapons systems with complex, low-frequency bending dynamics. For manned large space-based systems, such as the International Space Station, in addition to gravity gradient, control system, and deployment or docking forces, crew disturbance and the requirement to contain gas pressure comparable to 1 atm create vibrations that can affect delicate experiments being conducted onboard.[1] When disturbed, such structures are likely to vibrate for some considerable time because of their low-frequency modes and small inherent damping.

The absence of some energy loss mechanisms in space, such as aerodynamic damping, lead to structures with very low energy dissipation mechanisms. Although this can be alleviated with numerous passive-damping mechanisms, in some cases these will not be appropriate because of weight, structural, or environmental considerations. For example, viscoelastic materials, which provide damping over a wide frequency range, are often unsuitable for the space environment because of the outgassing[2] that occurs in these materials and the weight penalty they present. Other devices such as proof mass dampers can provide large amounts of damping with a small increase in mass, but only for a narrow frequency range.[3] For cases where no passive damping enhancement mechanism exists and low structural rigidity is present, active control can be used to attempt to meet the performance specifications. Although active control increases the complexity of the spacecraft, it does not necessarily require a large change in mass.

Piezoelectric materials are excellent candidates for the role of sensors and actuators for active vibration control of flexible structures. Piezoelectricity is a phenomenon that occurs in certain classes of anisotropic crystals subjected to changes in mechanical deformation.[4] By applying mechanical deformations to these crystals, electric dipoles are generated, and a potential difference develops that is contingent upon the changing deformations. Conversely, they also produce mechanical strain when an electric field is applied across them. Piezoelectric materials are, therefore, capable of acting as either a sensing or actuating element, or both.

In Ref. 5 an analytic model of the mechanical coupling of segmented lead zirconium titanate ceramic, a type of piezoelectric material when bonded to a one-dimensional elastic substructure, was developed. The model was experimentally verified using simple control experiments of small laboratory test articles. These analytical models have since been expanded to two-dimensional structures to investigate static[5] and dynamic[6–9] deformation of flat plates incorporating multiple patches of piezoelectric actuators. The desire to have a large level of robustness in control of aerospace structures and the availability of a number of sensors and actuators in flexible structures leads to the use of robust multivariable controllers, such as linear quadratic Gaussian (LQG) and H_∞ (Ref. 10).

The modeling of the static and dynamic response of piezolaminated shells with spatially discrete sensors and actuators has also been accomplished using finite element analysis.[11,12] The amount of strain and curvature induced by the piezoelectric actuators have been verified experimentally; however, in these studies no attempts were made to design control laws in order to investigate vibration suppression of flexible modes of a shell structure using piezoelectric ctuators. In addition, the effectiveness of H_∞ control design methodology in vibration suppression of flexible modes of curved plate components of flexible structures incorporating piezoelectric actuators has not been explored and compared with LQG control schemes.

The objective of this paper is to design and implement multivariable high-authority controllers experimentally for curved plate components of flexible structures. A test specimen, a curved plate, will be described. This test article was then available to be used as a testbed for various control strategies that can take advantage of continuously distributed piezoelectric actuators. It is not attempted to develop an analytical model for the curved plate incorporating piezoelectric actuators. Rather the aim is to identify a model in testing and then to use the model to design multivariable LQG and H_∞ controllers for vibration suppression of flexible modes of the curved plate with free-free-free-free boundary conditions.

Experimental Setup

The test structure consists of a curved plate ($30 \times 20 \times 0.3$ cm), made using aluminum. The flexibility of a curved plate is different in each direction, and this particular type of structural element can be found in every aerospace structure. To avoid fundamental control limitations imposed by using fewer actuators than important modes, at least as many control actuators as important modes should be used.[13] Therefore two piezoelectric actuators were needed. The test

Received 12 May 1999; presented as paper 99-3960 at the AIAA Guidance, Navigation, and Control Conference, Portland, OR, 9–11 August 1999; revision received 1 April 2000; accepted for publication 17 July 2000.

*Research Assistant, Dynamics and Control Research Group; currently System Designer, Virtek Engineering Sciences, Inc., 1 Bedford Road, Unit 5, Toronto, Ontario M5R 2J7, Canada. Member AIAA.
†Head, Mechanical Engineering, Oxford Road.
‡Head of School, Design, Engineering, and Computing.

Table 1 Elastic and geometric properties for the curved plate and piezoelectric actuators

Material property	Value
Plate bending modulus E_{pe}	70 Gpa
Piezo modulus E_{pe}	63 Gpa
Plate thickness t_p	3 mm
Piezo thickness t_{pe}	0.25 mm
Plate length L_{xp}	30 cm
Piezo length L_{xpe}	7 cm
Plate width L_{yp}	20 cm
Piezo width L_{ype}	2.5 cm

Table 2 Calculated and measured frequencies of the first three flexible modes of the curved plate

	Frequencies, Hz		
Mode	FEM	Exp.	Error, %
First (torsional)	112.30	107.75	4
Second (bending)	267.95	255.34	4
Third (bending)	342.70	315.7	8

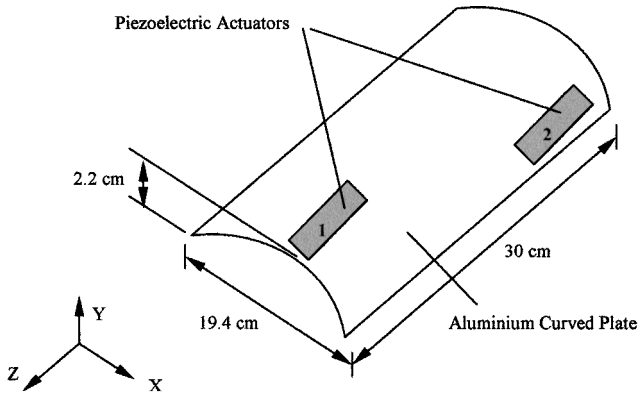

Fig. 1 Sketch of the curved plate incorporating two piezoelectric actuators (not to scale).

article was tested in a free-free-free-free configuration to approximate the actual space conditions, which would be encountered by components deployed in satellites or other space-based structures.

An overview diagram of the test specimen is shown in Fig. 1. The relevant dimensions and other data are given in Table 1. Actuator locations were determined by considering the effect of the piezoelectric induced strains on the mode shapes. High modal controllability is achieved by a piezoelectric actuator when it is placed in an area of high modal strain. Therefore, to choose locations for the piezoelectric actuators the bending strain contours of the first three modes were examined. The strain contour and deformation plots were obtained using ABAQUS finite element analysis software and plotted using PATRAN, as shown in Figs. 2a–2i. Examining the bending strain contours, it was apparent that the actuators should have been placed in the locations that were already shown in Fig. 1. The two piezoelectric actuators, PI Ceramic PIC 151 (charge constant, $d_{31} = -210 \times 10^{-12}$ mV^{-1}), were attached to both sides of the surface of the plate using a thin layer of conductive epoxy glue, and then the plate was grounded to Earth. The dimensions of the actuators are also given in Table 1.

The plate was then hung in a free-free-free-free configuration using two very thin rubber bands as shown in Fig. 3. Finally, a shaker, used as the disturbance source, was placed under the plate and connected to the specimen through a stinger rod and a force gauge (Fig. 3). This arrangement allowed the curved plate to be well isolated from the surrounding laboratory environment, allowing for accurate measurements of the frequency response of the system. The sensors, two high-impedance accelerometers, were placed at the center of the locations of the two actuators to provide collocated sensor-actuator configuration.

A table of calculated and measured frequencies of the first three flexible modes is given in Table 2. The calculated values were determined using ABAQUS finite element software, and the experimental values were obtained using a spectrum analyser with white-noise excitation.

As can be seen, the finite element model agrees fairly well with the experimental measurements for the first three flexible modes.

System Identification Using Hankel Singular Value Decomposition

A linear dynamical system can be represented by a discrete-time state-space model of the form

$$\boldsymbol{x}(k+1) = A\boldsymbol{x}(k) + B\boldsymbol{u}(k), \qquad \boldsymbol{y}(k) = C\boldsymbol{x}(k) + D\boldsymbol{u}(k)$$
$$k = 0, 1, \ldots \quad (1)$$

where $\boldsymbol{x}$, $\boldsymbol{u}$ and $\boldsymbol{y}$ are the state ($n \times 1$), control ($nu \times 1$), and output ($ny \times 1$) vectors, respectively. Because experimental data are discrete in nature (they are recorded in a digital computer), this set of equations forms the basis for the system identification of linear, time-invariant, dynamical systems.

Let a unit pulse input be defined by $u_i(0) = 1$ ($i = 1, 2, \ldots, r$) and $u_i(k) = 0$ ($k = 1, 2, \ldots$) be substituted into Eqs. (1). This results in a unit pulse-response matrix $h(ny \times nu)$ as follows:

$$h_0 = D, \qquad h_1 = CB, \qquad h_2 = CAB, \ldots, \qquad h_k = CA^{k-1}B \quad (2)$$

These sequences are known as Markov parameters.[14] The aim of system realization is to determine a state-space representation, a triple A, B, C], such that it generates a new Markov parameter sequence that approximates the original one. Notice that D is equal to h_0.

Now assume the length of the measured sequence is $N + 1$, i.e., $\{h_0, h_1, h_2, \ldots, h_N\}$. The Hankel matrix ($rh \times ch$) is defined as

$$\Gamma = \begin{bmatrix} h_1 & h_2 & h_3 & \cdots & h_N \\ h_2 & h_3 & h_4 & \cdots & 0 \\ h_3 & h_4 & h_5 & \cdots & 0 \\ \vdots & \vdots & \vdots & \ddots & \vdots \\ h_N & 0 & 0 & \cdots & 0 \end{bmatrix} \quad (3)$$

Performing singular value decomposition on the Hankel matrix Γ yields

$$\Gamma = U\Sigma V = \begin{bmatrix} U_1 & U_2 \end{bmatrix} \begin{bmatrix} \Sigma_1 & 0 \\ 0 & \Sigma_2 \end{bmatrix} \begin{bmatrix} V_1 \\ V_2 \end{bmatrix} \quad (4)$$

where Σ_1 has dimension $n \times n$ (i.e., the system order) and the entries of Σ_2 are nearly zero. The matrices U_1 and V_1, which have ny and nu columns, respectively, can be partitioned into three matrix blocks:

$$U_1 = \begin{bmatrix} U_{11} \\ U_{12} \\ U_{13} \end{bmatrix}, \qquad V_1 = \begin{bmatrix} V_{11} \\ V_{12} \\ V_{13} \end{bmatrix} \quad (5)$$

where the matrices U_{11}, U_{12}, U_{13}, and V_{11} are defined as

$$U_{11} = U_1(1 : rh - ny, 1 : n), \qquad U_{12} = U_1(1 : ch - nu, 1 : n)$$
$$U_{13} = U_1(rh - ny + 1 : rh, 1 : n)$$
$$V_{11} = V_1(1 : ch - nu, 1 : n) \quad (6)$$

Then a discrete state-space realization is computed as[15]

$$A = \Sigma_1^{-\frac{1}{2}} \bar{U} \Sigma_1^{\frac{1}{2}}, \qquad B = \Sigma_1^{\frac{1}{2}} V_{11}, \qquad C = U_{11}\Sigma_1^{\frac{1}{2}}, \qquad D = h_0 \quad (7)$$

where

$$\bar{U} = \begin{bmatrix} U_{11} \\ U_{12} \end{bmatrix}^T \begin{bmatrix} U_{12} \\ U_{13} \end{bmatrix} \quad (8)$$

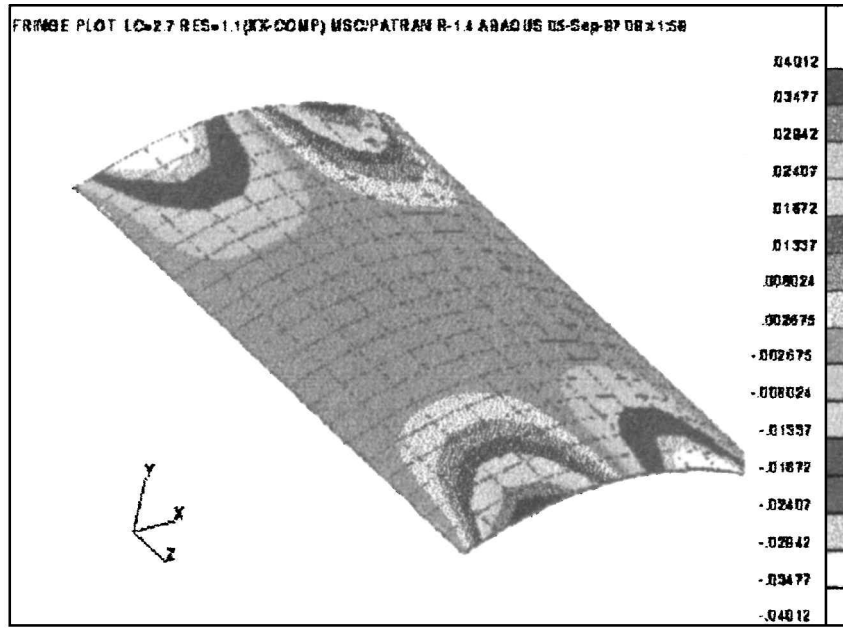

Fig. 2a Strain contours σ_{xx} of the curved plate for the first flexible mode (first torsional mode).

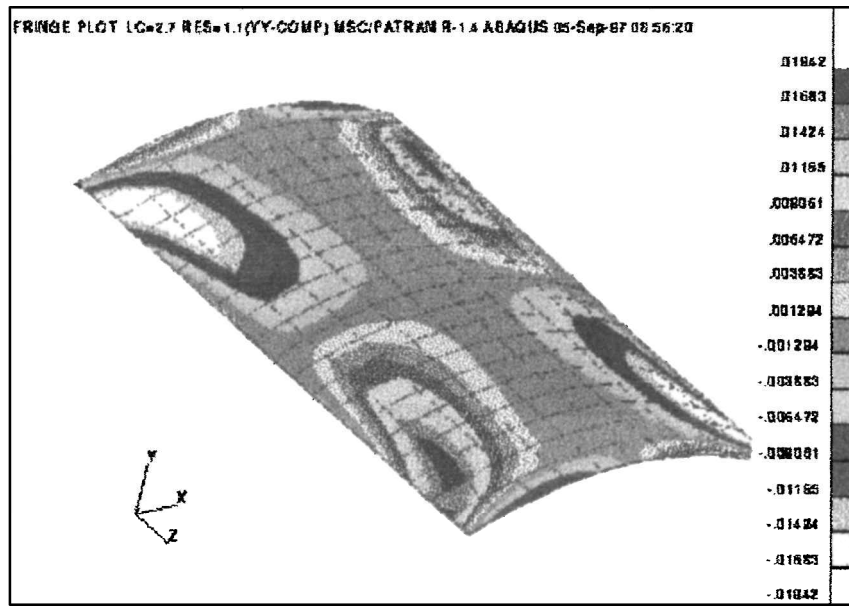

Fig. 2b Strain contours σ_{zz} of the curved plate for the first flexible mode (first torsional mode).

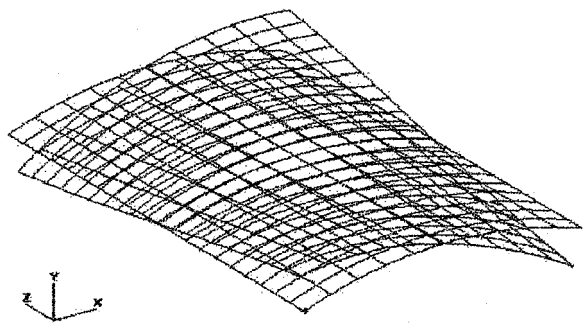

Fig. 2c Deformation of the curved plate for the first flexible mode (first torsional mode).

A special state-space form can always be obtained in which the input-to-state and state-to-output effects have a balanced performance.[16] Such realizations are termed *internally balanced.*[16] The realization $A, B, C]$ explained here is an internally balanced system, which yields a system as well-conditioned as possible.[17] Meanwhile it can be proved that the realization obtained as in Eq. (7) will represent a stable discrete-time system.[15] The Markov parameters of a system are determined by applying inverse discrete Fourier transform to frequency response data.

Closed-Loop Velocity Feedback Experiments

In this section velocity feedback controller will be examined. The velocity signals will be provided using two accelerometers, located at the center of the location of the actuators, with analog integrators. For this simple control philosophy no mathematical model of the structure is required. Collocated velocity signals will be fed back to actuator 1 and actuator 2, and the closed-loop frequency response will be recorded and compared with the open-loop frequency response.

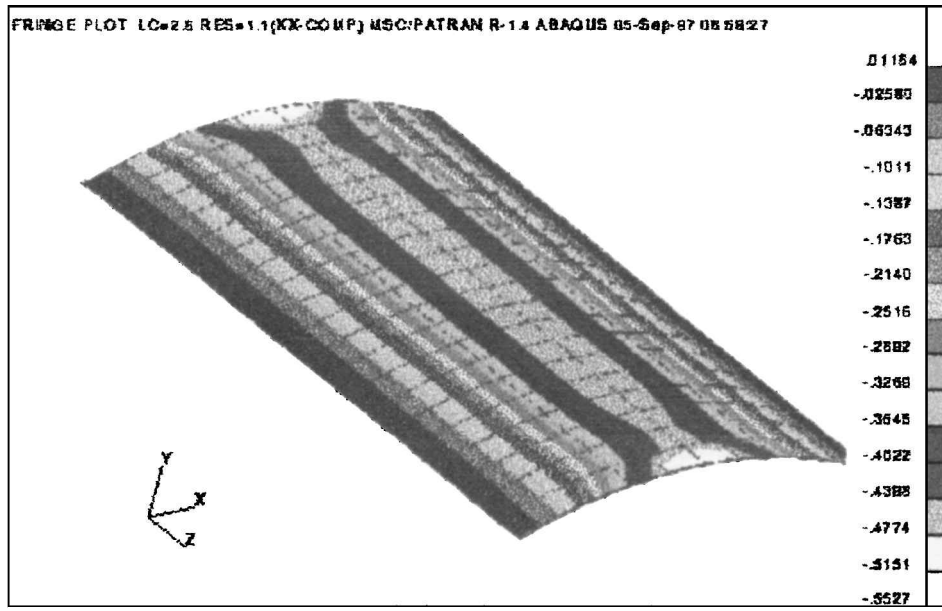

Fig. 2d Strain contours σ_{xx} of the curved plate for the second flexible mode (first bending mode).

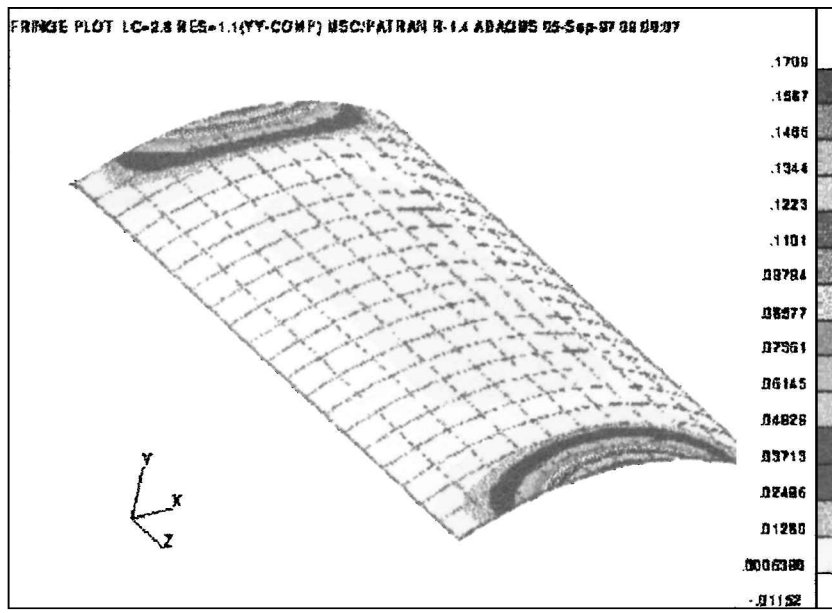

Fig. 2e Strain contours σ_{zz} of the curved plate for the second flexible mode (first bending mode).

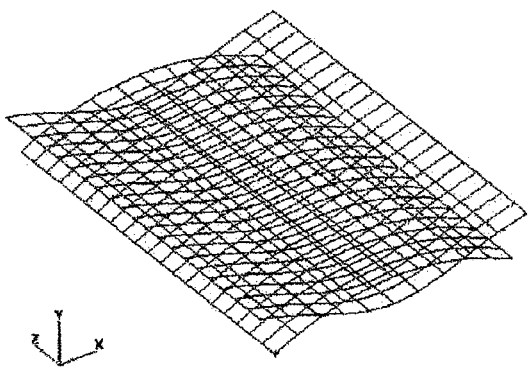

Fig. 2f Deformation of the curved plate for the second flexible mode (first bending mode).

To obtain a measure of the closed-loop performance in the pattern of an external disturbance, the structure was excited using a shaker with a random input signal from a spectrum analyzer. The feedback system is shown in Fig. 4. The exciter was placed at approximately the quarter span because at this location the disturbance source was found to excite the test structure most effectively. The feedback gain was then slowly increased until instability appeared in the system. As this was being done, particular care was taken to identify any possible onset of instability present in the system. The closed-loop transfer function was then obtained and stored. The open- and closed-loop frequency responses of the curved plate, containing rigid-body and flexible modes, using a logarithmic scale are shown in Fig. 5. Because of 1-*g* gravity environment, zero-frequency rigid-body modes are stiffened to nonzero frequencies in a manner similar to the simple pendulum.

Only small improvements in damping (less than 5-dB vibration attenuation in the flexible modes) were achieved in the system using

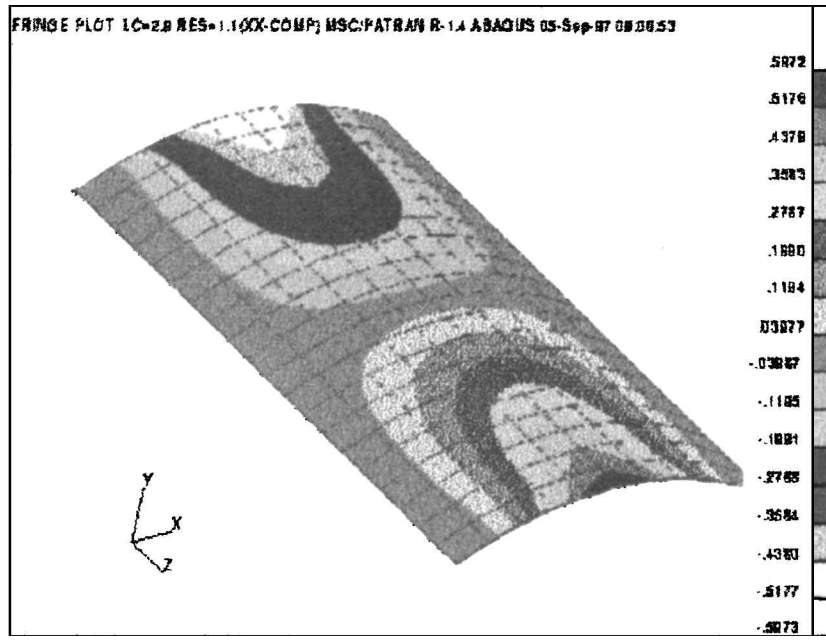

Fig. 2g Strain contours σ_{xx} of the curved plate for the third flexible mode (second bending mode).

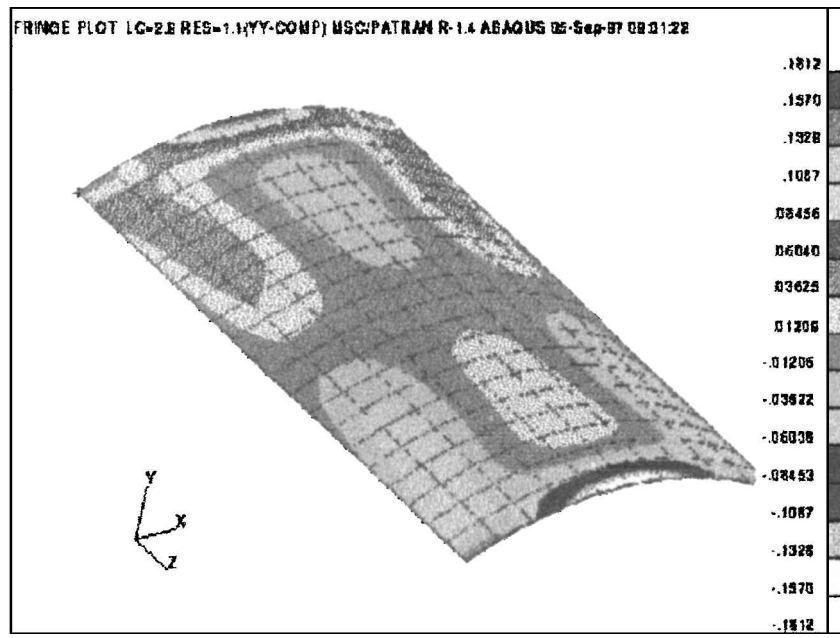

Fig. 2h Strain contours σ_{zz} of the curved plate for the third flexible mode (second bending mode).

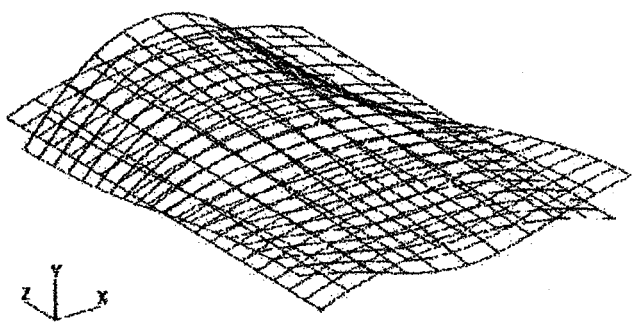

Fig. 2i Deformation of the curved plate for the third flexible mode (second bending mode).

two single-input/single-output velocity feedback controllers. Also, the first flexible mode is hardly observable.

Up to this point, only velocity feedback has been used in the experiment, and therefore it is necessary to examine the effect of multivariable controllers on the structure. However because no mathematical model was assumed to be available for the structure; first a parametric model is identified for the system experimentally using Hankel singular values decomposition (HSVD) explained before.

System Identification of the Curved Plate Test Structure

The purpose of this section is to construct a state-space model from impulse response data. The system identification experiments are conducted using a real-time dual Pentium 200-MHz computer operating at a 2000-Hz sampling rate for accurate measurement up to 500 Hz.

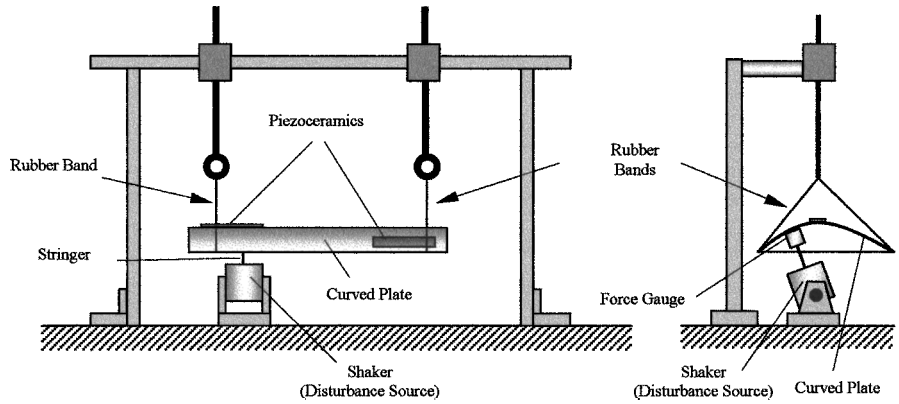

Fig. 3 Curved plate in free-free-free-free configuration (not to scale). Accelerometers are not shown.

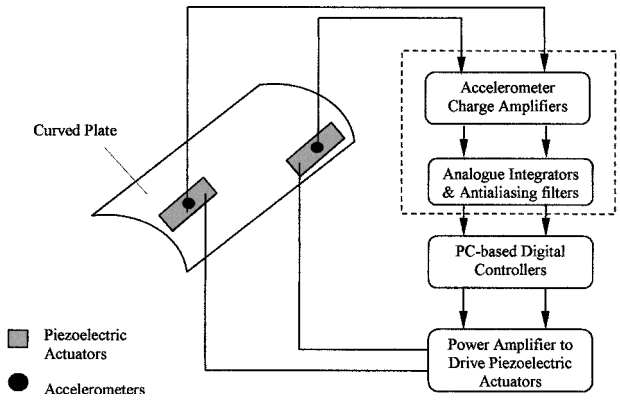

Fig. 4 Measurement schematic for single-input, single-output tests (not to scale).

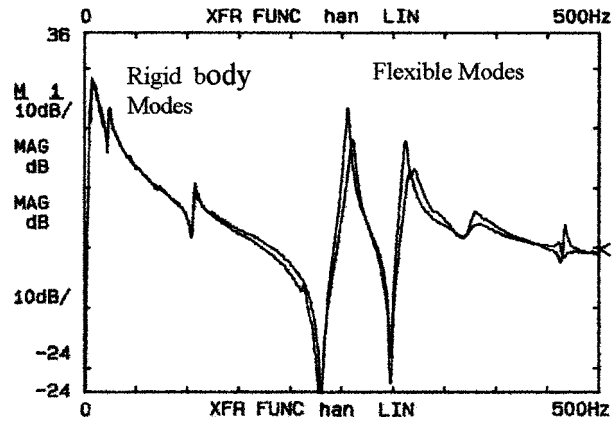

Fig. 5 Experimental open- and closed-loop transfer functions from the accelerometer 1 to excitation on the shaker showing the first three modes of the curved plate (log scale).

Measured frequency response data were collected using VirtualBench Suite software[18] and a Lab-PC-1200 data acquisition (DAQ) card via single-input, multi-output tests, i.e., exciting each actuator as well as the shaker with band-limited white noise and computing the frequency responses to all of the sensor channels. The multi-input, multi-output (MIMO) tests were performed in the frequency range 30–500 Hz with 2000-Hz sampling rate. This frequency range was selected so as to avoid-low frequency rigid-body modes. The reason for this was that a number of multivariable controllers were designed using a model including rigid-body modes, but because of the zero-pole cancellation of extremely lightly damped rigid-body modes that occurred in the design procedure satisfactory results were not obtained. This is an important issue of which one should be aware. Thus, it was decided to limit the bandwidth of the excitation signal using a band-limited white noise. The measured data were then transferred to MATLAB® software to calculate unit impulse responses (the Markov parameters) using the inverse discrete Fourier transform (IDFT), and finally the HSVD method was used to realize an overparameterized state-space model for the system.

Using the Markov parameters, different models of different orders were computed using the HSVD algorithm. When compared with the data, larger models were more accurate. However to carry out control design procedure, a low-order model was required. A number of controllers were designed, and their closed-loop performance was tested; it was found that the minimum order necessary to properly design control laws was 25. A comparison between the measured and modelled frequency responses is shown in Fig. 6. The comparison in the figure shows good agreement between the frequency responses throughout the entire frequency range in all channels. Although there are some observable mismatches between the model and the data, the model captured the general shapes of measured frequency responses of the modes of interest in all channels.

Control Design

In this section the model obtained using HSVD will be used to design multivariable controllers for vibration attenuation of the curved plate test specimen. LQG and H_∞ controllers will be designed, and their effectiveness will be investigated.

LQG Control Design and Experimental Results

The LQG compensator contains the full-state feedback linear quadratic regulator (LQR)[10] and a Kalman filter[19] as the state estimator. The state cost for the LQR compensator is chosen as the sum of the output $\boldsymbol{y}$ rms response squared, and the control cost is chosen to be the sum of the control $\boldsymbol{u}$ rms response squared. The total performance index J is then defined to be

$$J = \int_0^\infty \bar{\boldsymbol{y}}^T \bar{\boldsymbol{y}} + \rho \bar{\boldsymbol{u}}^T \bar{\boldsymbol{u}}]\,\mathrm{d}t = \int_0^\infty \boldsymbol{x}^T Q \boldsymbol{x} + \rho \boldsymbol{u}^T R \boldsymbol{u}]\,\mathrm{d}t$$

$$Q = C/y_{\max}]^T\ C/y_{\max}], \qquad R = I/u_{\max}^2 \tag{9}$$

where ρ is a design parameter to weight relative state to control cost; the lower the value of ρ, the higher the value of compensator gain and consequently the higher the control energy. The physical outputs $\boldsymbol{y}$ and the inputs $\boldsymbol{u}$ are normalized by their maximum values to calculate the scaled outputs $\bar{\boldsymbol{y}}$ and inputs $\bar{\boldsymbol{u}}$. The value of $y_{\max}$ is selected to be 0.5 V, i.e., is the maximum expected sensor charge amplifier outputs caused by the disturbance source. The value of $u_{\max}$ that is generated by the DAQ card was selected to be ± 2 V, because the amplifier gain (100 to generate a maximum ± 200 V) was already included in the model.

Using this methodology, control laws were designed using two piezoelectric actuators and two accelerometers. The MIMO designs proceeded by selecting process noise, the effect of external disturbances, and measurement noise intensity and design parameter ρ based on engineering judgement through an iterative procedure.

The controllers designed were of order of 25 because the order of the model was chosen to be 25. The order of the controllers were reduced to 20 using the relative error Schur model order reduction[20,21] for two important reasons:

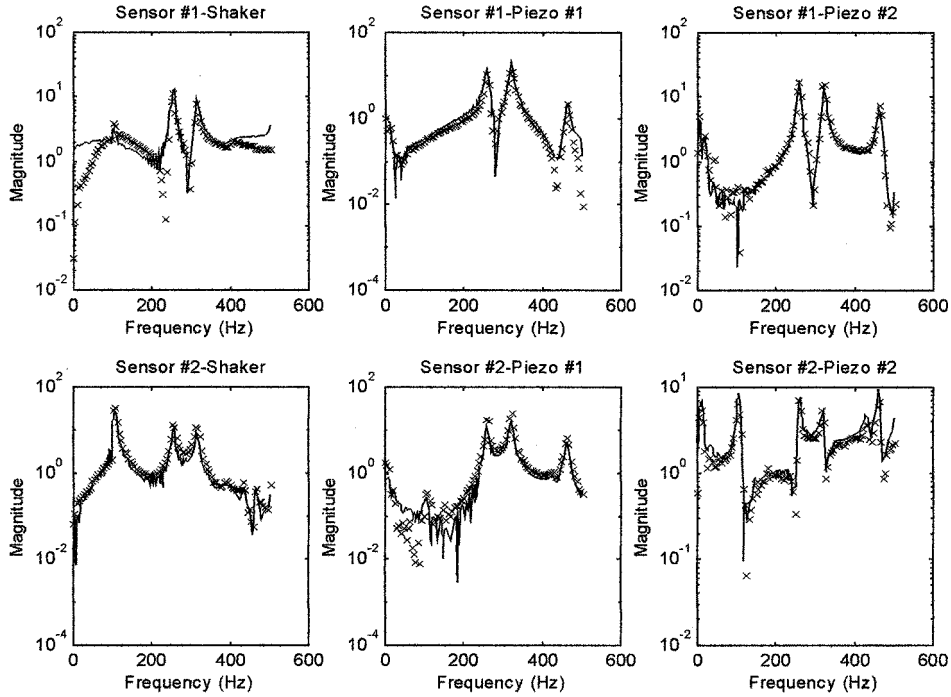

Fig. 6 Measured and identified frequency responses of the curved plate. The frequency response data were obtained using VirtualBench Suite via single-input, multi-output tests: ×, measured, and ——, identified.

1) To conduct closed-loop experiment using a PC-based real-time controller at the speed of 2000-Hz sampling rate, it was desired not to have a controller with more than 20 states.

2) To remove unnecessary and potentially harmful dynamics, such as inverted zeros appearing in the compensator as poles. These poles are those near to the $j\omega$ axis, which causes difficulty in real-time implementation because they might appear as unstable poles. This is an important issue because a number of controllers failed to perform as a result of instabilities occurring during real-time implementation.

The first step of the testing procedure for a given control law was to check if the controller itself were stable by examining its eigenvalues. Even for stable systems, optimal approaches often lead to unstable compensators if the performance requirements are sufficiently demanding. The fundamental problem with implementing unstable compensators is that resulting closed-loop systems are conditionally stable. Therefore only if the controller were found to be stable, the loop would then be physically closed, and the excitation level could be slowly increased. In addition, the controllers were internally balanced to provide well-conditioned controllers for digital implementation.[17]

The LQG compensators with measurement noise intensity less than 50 were found to be unstable. However, for measurement noise intensity of greater than 50, the controllers were stable, and in fact they had good repeatability characteristics. The singular values bode plot of the LQG controller designed (full order and truncated) using $\rho = 10^{-2}$ process noise equal to 1 and measurement noise intensity equal to 10^2 is shown in Fig. 7. The figure shows the high gain of the control bandwidth and the roll-off region to avoid destabilizing high-frequency mode. Being stable, this controller produced the best performance throughout the closed-loop experiments. The experimental closed-loop performance can be seen in Fig. 8 for the LQG controller. Quantitatively, the vibration attenuation was obtained as 3, 7, 15 dB in the first three modes of vibration, respectively. In the figure the frequency response obtained using sensor #2 is shown in order to examine performance of the controller in the first mode as well as the second and third modes.

As can be noticed, the closed-loop performance in the first mode is not as good as in the second and particularly the third modes. Examining Fig. 5 indicates that the first mode was not observable from sensor 1. Therefore, there is not enough information available to the controller regarding the first mode. In addition, the level of attenuation of the third mode is higher than that of the second mode.

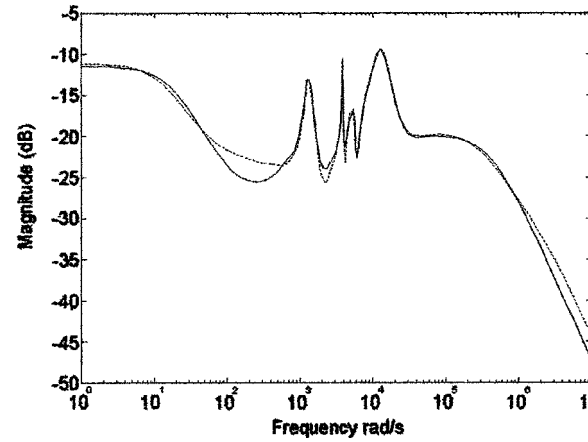

Fig. 7 Full-order and truncated LQG compensators maximum singular value plots, with $\rho = 10^{-2}$ and noise intensity equal to 10^2: - - - -, full order, and ——, truncated.

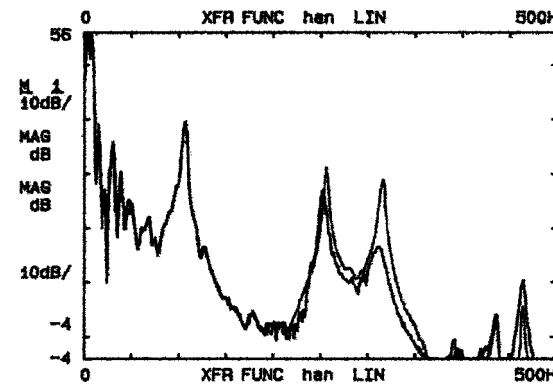

Fig. 8 Experimental open- and closed-loop frequency response of the curved plate from disturbance source to sensor 2 for the multivariable LQC control design with $\rho = 10^{-2}$ and the measurement noise intensity at 10^2.

The reason for this can be explained by examining Fig. 2. Sections 2d–2f of the figure, which indicate that the plate vibrates along the x direction (first bending mode) as a result of the maximum stress in the middle along the z direction, whereas sections 2g–2h show that the third mode (second bending mode) vibrates along both the x and z direction. However, the length of the piezoelectric actuator is nearly three times its width. This limits the authority of the actuator along the x direction.

Throughout the experiments visual inspection of the test model was performed to indicate any severe damage to the piezoelectric actuators as a result of the curvature of the plate. In addition, the piezoelectric actuators were electrically tested to examine if they were short-circuited.

H_∞ Mixed Sensitivity Design and Experimental Results

To begin designing the H_∞ controller using mixed sensitivity approach, the three weighting functions W_1, W_2, W_3 should be determined.[20,21] The performance weight W_1 for the vibration suppression is a low-pass filter that rolls off after 3000 rad/s. This specifies that vibration suppression is desired for the frequency dynamics less than 500 Hz. The multiplicative uncertainty weight W_3 is chosen as a high-pass filter with 20% error in the model, with a break frequency of approximately 100 rad/s. This will ensure that the system will have sufficient stability margin to tolerate variations in the model such as those might arise from unmodelled structural modes at and beyond this frequency. The final weight W_2 determines the shape of the controller in the frequency domain. Because it is important for the controller to roll off at higher frequencies, the weight increases sharply throughout the region of interest. High-frequency roll off of the controller is necessary so that unmodeled dynamics are not destabilized by the active control. However, a number of frequency-dependent functions were attempted without any success in finding an H_∞ controller. Thus, it was decided to choose a constant value of two to limit the gain of the controller. Because the model has two inputs and two outputs, two frequency-dependent functions are necessary for each weighting function. Taking the factors just noted into account, the weighting functions W_1, W_2, W_3 were chosen to be

$$W_1(s) = \begin{bmatrix} \dfrac{(s/10{,}000+1)}{(s/3000+1)} & 0 \\ 0 & \dfrac{(s/10{,}000+1)}{(s/3000+1)} \end{bmatrix} \gamma$$

$$W_2(s) = 2 \times I$$

$$W_3(s) = \begin{bmatrix} \dfrac{0.2(s/100+1)}{(s/400+1)} & 0 \\ 0 & \dfrac{0.2(s/100+1)}{(s/400+1)} \end{bmatrix} \qquad (10)$$

The real parameter γ is used as a design "knob" that is iteratively increased until one of the design criteria is violated and no solution exists for any larger γ.

After a few iterations the optimum value of γ was found to be 9.534×10^{-3}. The H_∞ solution results in a 29th-order controller. (The order of the model was found to be 25.) The relative error Schur model order reduction method[20,21] was used to reduce the order of the controller to 20. The full-order and truncated controller maximum singular values plot is shown in Fig. 9, indicating the validity of the model order reduction. The figure also shows the high gain of the control bandwidth and the roll-off region to avoid destabilizing high-frequency modes. This controller was stable when applied to the test structure. The controller was again internally balanced to provide well-conditioned controllers for digital implementation.

Experimental open- and closed-loop frequency responses of the curved plate test specimen for the H_∞ controller designed are shown in Fig. 10. The figure illustrates that damping was introduced into the first three flexible modes of the structural by the H_∞ controller designed using the mixed sensitivity approach. Quantitatively, the magnitude of the closed-loop frequency response was reduced from that of the open-loop system by approximately 3, 7, and 12 dB in the first three modes. The figure shows that the controller has succeeded

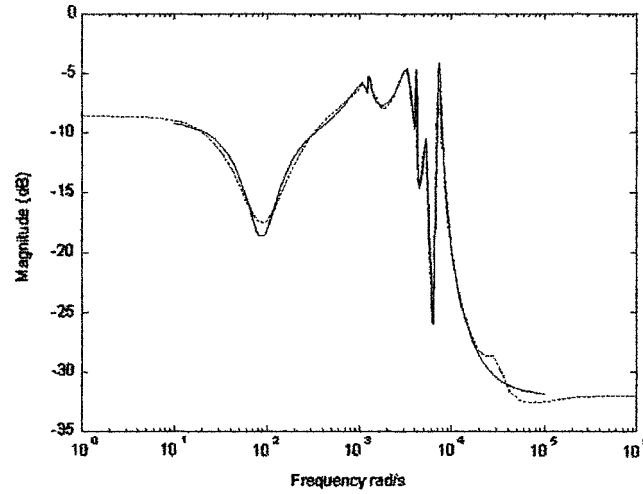

Fig. 9 Full-order and truncated H_∞ maximum singular value plot: – – –, full order, and ——, truncated.

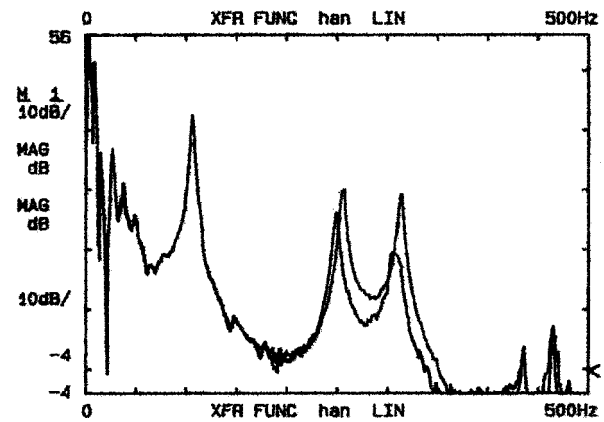

Fig. 10 Experimental open- and closed-loop frequency response of the curved plate from disturbance source to sensor 2 for the multivariable H_∞ control design.

in reducing the resonant behavior of the structural modes showing the capability of the strain actuation, which provides direct control of the strain in the structure.

Analysis of Control Limitations

The closed-loop testing proved to be successful with control laws demonstrating vibration suppression of the curved plate. However, there were major limitations: 1) the authority of the actuators as a result of the difference in their dimensions along the x and z direction and 2) the choice of sensor type/location, which limited the observability of the systems.

The authority of the actuators can be increased by increasing the coverage of the piezoelectric. The curved plate was only covered with two actuators. If fuller coverage of the curved plate were obtained by grouping a number of actuators, that would certainly increase the authority.

The second performance limitation was caused by the inappropriate choice of sensor and/or actuator location. Apparently acceleration sensor and induced strain actuator collocation was not a proper choice to improve the observability of this particular structure. If piezoelectric film were used instead of inertial sensors (accelerometers), that would probably improve the observability resulting in having much better controller and consequently higher vibration attenuation.

Conclusions

In this paper vibration suppression of flexible modes of a curved plate structure incorporating two piezoelectric actuators in free-free-free-free configuration has been investigated. Because it was

assumed no mathematical model was available for this particular structure, HSVD was used to obtain a MIMO state-space representation of the structure using impulse response data. The impulse response data were obtained by applying the inverse discrete Fourier transform to frequency response data of the system collected using VirtualBench Suite and Lab-PC-1200 DAQ card via single-input, multi-output tests. Band-limited white noise (30–500 Hz) was used throughout the system identification procedure to avoid rigid-body modes in the control design process. The system identification procedure was able to capture the general shapes of the measured frequency responses. High-authority multivariable LQG and H_∞ controllers were designed. Controllers were internally balanced, and only stable controllers were implemented.

Although the level of vibration attenuation was not as much as expected, piezoelectric actuators with robust controllers have been used successfully to control the flexible modes of that particular structure. There were several factors, which limited performance. These include the authority of the piezoelectric actuators, optimal placement of actuators, and sensors and the choice of actuator/sensor complement.

References

[1]Nurre, G. S., Ryan, R. S., Scofield, H. N., and Sims, J. L., "Dynamics and Control of Large Space Structures," *Journal of Guidance, Control, and Dynamics*, Vol. 7, No. 5, 1984, pp. 514–526.

[2]Chen, G.-S., and Wada, B. K., "Passive Damping for Space Truss Structures," AIAA Paper 88-2469, Aug. 1988.

[3]Politansky, H., and Pilkey, W. D., "Suboptimal Feedback Vibration Control of a Beam with a Proof-Mass Actuator," *Journal of Guidance, Control, and Dynamics*, Vol. 12, No. 5, 1989, pp. 691–697.

[4]Piezo Systems, Inc., *Interim Catalogue 2B*, Nov. 1997.

[5]Crawley, E. F., and Lazarus, K. B., "Induced Strain Actuation of Isotripic and Anisotropic Plates," *AIAA Journal*, Vol. 29, No. 6, 1990, pp. 944–951.

[6]Dimitriadis, E. K., Fuller, C. R., and Rogers, C. A., "Piezoelectric Actuators for Distributed Vibration Excitation of Thin Plates," *Journal of Vibration and Acoustics*, Vol. 113, No. 1, 1991, pp. 100–107.

[7]Miller, S. E., Oshman, Y., and Abramovich, H., "Modal Control of Piezolaminated Anisotropic Rectangular Plates Part1: Modal Transducer Theory," *AIAA Journal*, Vol. 34, No. 9, 1996, pp. 1868–1875.

[8]Miller, S. E., Oshman, Y., and Abramovich, H., "Modal Control of Piezolaminated Anisotropic Rectangular Plates Part 2: Control Theory," *AIAA Journal*, Vol. 34, No. 9, 1996, pp. 1876–1884.

[9]Sadri, A. M., Wynne, R. J., and Wright, J. R., "The Design and Implementation of Robust Strategies for Active Vibration Control," American Automatic Control Conf., Paper FP01-2, June 1998.

[10]Maciejowski, J. M., *Multivariable Feedback Design*, Addison Wesley Longman, Reading, MA, 1989, pp. 100–105.

[11]Pletner, B., and Abramovich, H., "Consistent Methodology for the Modeling of Piezolaminated Shells," *AIAA Journal*, Vol. 35, No. 8, 1997, pp. 1316–1326.

[12]Saravanos, D. A., "Mixed Laminate Theory and Finite Element for Smart Piezoelectric Composite Shell Structures," *AIAA Journal*, Vol. 25, No. 8, 1997, pp. 1327–1333.

[13]Lazarus, K. B., Crawley, E. F., and Lin, C. Y., "Fundamental Mechanisms of Aeroelastic Control with Control Surface and Strain Actuation," *Journal of Guidance, Control, and Dynamics*, Vol. 18, No. 1, 1995. pp. 10–17.

[14]Juang, Jer-Nan, *Applied System Identification*, Prentice–Hall, Upper Saddle River, NJ, 1994, pp. 70–72.

[15]Kung, S., "A New Identification and Model Reduction Algorithm via Singular Value Decomposition," *Proceedings of International Symposium on Circuit, System and Computers*, 1978, pp. 705–714.

[16]Balas, G. J., Doyle, J. C., Glover, K., Packard, A., and Smith, R., *μ-Analysis and Synthesis Toolbox Users's Guide*, The Math Works, Inc., Natick, MA, 1995.

[17]Chou, C. T., and Maciejowski, J. M., "System Identification Using Balanced Parameterisations," *IEEE Transactions on Automatic Control*, Vol. 42, No. 7, 1997, pp. 956–974.

[18]National Instruments, *Instrumentation Catalogue*, 1998, pp. 153–155.

[19]Gelb, A., *Applied Optimal Estimation*, MIT Press, Cambridge, MA, 1974, pp. 102–105.

[20]Chiang, R. Y., "Modern Robust Control Theory," Ph.D. Dissertation, Dept. of Electrical Engineering, Univ. of Southern California, Dec. 1988.

[21]Chiang, R. Y., and Safonov, M. G., *Robust Control Toolbox Users's Guide*, The Math Works, Inc., Natick, MA, 1992, pp. (2-60)–(2-80).

A. Chattopadhyay
Associate Editor